X-ray Reflectivity Characterization of ZnO/Al 2 O 3 Multilayers Prepared by Atomic Layer Deposition

6 AUTHORS, INCLUDING:

David C. Johnson
University of Oregon
274 PUBLICATIONS **2,664** CITATIONS

SEE PROFILE

Jeffrey W. Elam
Argonne National Laboratory
307 PUBLICATIONS **8,415** CITATIONS

SEE PROFILE

S.M. George
University of Colorado Boulder
183 PUBLICATIONS **8,341** CITATIONS

SEE PROFILE

X-ray Reflectivity Characterization of ZnO/Al₂O₃ Multilayers Prepared by Atomic Layer Deposition

J. M. Jensen, A. B. Oelkers, R. Toivola, and D. C. Johnson*

Department of Chemistry and Materials Science Institute, University of Oregon, Eugene, Oregon 97403

J. W. Elam and S. M. George

Department of Chemistry and Biochemistry, University of Colorado, Boulder, Colorado 80309-0215

Specular X-ray reflectivity (XRR) has been employed in the characterization of a novel series of ZnO/Al₂O₃ multilayer materials prepared by atomic layer deposition in a custom-built hot-wall reactor. All multilayers studied are approximately 1200 Å thick and consist of 1−128 ZnO/Al₂O₃ bilayer subunits. Reflectivity data are treated both qualitatively and quantitatively by computer-aided simulation and modeling. Surface roughness is observed to increase dramatically with increasing ZnO layer thickness. ZnO density is determined to be within 5% of bulk values, while the Al₂O₃ layers exhibit densities less than 80% of that expected for crystalline alumina. Thickness parameters determined by computer simulation correspond to deposition rates of 1.71 and 1.28 Å/reaction cycle for ZnO and Al₂O₃, respectively. XRR-determined thickness and density parameters are in clear quantitative agreement with analyses of single-component films by other techniques. Conventional and grazing-incidence X-ray diffraction show the ZnO layers to be polycrystalline above a critical layer thickness of approximately 10 Å. The Al₂O₃ layers are amorphous.

Introduction

Artificially layered materials often exhibit characteristic properties which are not observed in the constituent layer materials alone.[1] Recent years have seen the preparation of multilayer materials with a diverse array of technologically important properties including soft X-ray reflectivity,[2,3] giant magnetoresistance,[4−6] perpendicular magnetic anisotropy,[7] enhanced mechanical hardness,[8] and high-temperature stability.[9,10] In most instances a high-quality multilayer must be prepared to exhibit the desired property. Factors contributing to multilayer quality include interfacial roughness, interdiffusion between layers, layer-to-layer consistency, and layer conformality. The preparation of high-quality multilayer materials requires a preparation method by which the above factors can be precisely controlled.

Atomic layer deposition (ALD) is a potentially powerful method for preparing high-quality multilayer films.[11−13] The advantages of ALD techniques over traditional physical or chemical vapor deposition methods include accurate control of film thickness, large-scale uniformity, highly conformal layering, and sharp interfaces.[12−14] Attesting to the versatility of the technique is the vast library of materials which are accessible by ALD methods, ranging from single elements[15] to compound semiconductors[16] to oxides, nitrides, and sulfides.[12−14] In addition to the preparation of high-quality thin films, ALD has been used to create high-quality multicomponent multilayer films.[11]

The preparation of high-quality multilayers by atomic layer deposition requires a robust means of characterization to ensure that key physical parameters such as layer thickness, interfacial quality, and density are well-controlled. Direct methods of characterization, such as electron microscopy imaging, are necessarily destructive and only provide information regarding a very small area of the sample. The accuracy of indirect characterization methods such as ellipsometry rely on the accuracy of user-defined material parameters such as refractive index, which are often assumed or entirely

* To whom correspondence should be addressed.

(1) DiSalvo, F. J. In *Advancing Materials Research*; Psaras, P. A., Langford, H. D., Eds.; National Academy Press: Washington, D.C., 1987; pp 161−176.

(2) Cilia, M.; Verhoeven, J. *J. Appl. Phys.* **1997**, *82*, 4137−4142.

(3) Ulyanenkov, A.; Matsuo, R.; Omote, K.; Inaba, K.; Harada, J.; Ishino, M.; Nishii, M.; Yoda, O. *J. Appl. Phys.* **2000**, *87*, 7255−7260.

(4) Ratzke, K.; Hall, M. J.; Jardine, D. B.; Shih, W. C.; Somekh, R. E.; Greer, A. L. *J. Magn. Magn. Mater.* **1999**, *204*, 61−67.

(5) Baibich, M. N.; Broto, J. M.; Fert, A.; Nguyen Van Dau, F.; Petroff, F.; Eitenne, P.; Creuzet, G.; Friederich, A.; Chazelas, J. *Phys. Rev. Lett.* **1988**, *61*, 2472−2475.

(6) Pape, I.; Hase, T. P. A.; Tanner, B. K.; Wormington, M. *Physica B* **1998**, *253*, 278−289.

(7) Carcia, P. F. *J. Appl. Phys.* **1988**, *63*, 5066−5073.

(8) Sproul, W. *Vacuum* **1998**, *51*, 641−646.

(9) Ramaswamy, P.; Seetharamu, S.; Varma, K. B. R.; Rao, K. J. *Compos. Sci. Technol.* **1997**, *57*, 81−89.

(10) Andritschky, M.; Cunha, I.; Alpuim, P. *Surf. Coat. Technol.* **1997**, *94−95*, 144−148.

(11) Kumagai, H.; Toyoda, K.; Kobayashi, K.; Obara, M.; Iimura, Y. *Appl. Phys. Lett.* **1997**, *70*, 2338−2340.

(12) Leskela, M.; Ritala, M. *J. Phys. IV* **1999**, *9*, 837−852.

(13) Ritala, M. *Appl. Surf. Sci.* **1997**, *112*, 223−230.

(14) Ott, A. W.; Klaus, J. W.; Johnson, J. M.; George, S. M. *Thin Solid Films* **1997**, *292*, 135−144.

(15) Klaus, J. W.; Ferro, S. J.; George, S. M. *Thin Solid Films* **2000**, *360*, 145−153.

(16) Suntola, T.; Simpson, M. *Atomic Layer Epitaxy*; Chapman and Hall: New York, 1990.

unknown. X-ray reflectivity (XRR), or low-angle X-ray diffraction, provides nondestructive, accurate characterization of thin films and multilayers.[3,17,18] X-ray reflectivity probes the intensity of scattered X-rays at small angles, providing information about film thickness, roughness, and density. The fundamental framework for quantitative interpretation of X-ray reflectivity data was derived in the 1950s by Parratt,[19] though the task of carrying out the necessary recursion calculation by hand limited its application initially to simple systems.[20,21] The advent of high-performance desktop PCs drastically reduced the requisite calculation time, allowing simulated reflectivity for complicated multilayer systems to be carried out in a matter of seconds.[22] Further advances in processor speed have enabled the implementation of efficient autofitting algorithms, providing a more objective alternative to cumbersome "guess and check" techniques.[3,23] Increasing demand for reflectivity analyses in industry has spurred the development of several commercial software packages which provide an efficient and accurate means of extracting thickness, density, and interfacial quality from measured reflectivity curves.

We present an X-ray reflectivity study of a series of ZnO/Al₂O₃ multilayers prepared in a custom-built hot-wall reactor using well-established organometal-based precursor chemistries for ZnO[24-27] and Al₂O₃.[14,28] We discuss interfacial quality, layer-to-layer uniformity, and control over deposition conditions qualitatively in light of features in measured reflectivity curves. By computer-assisted quantitative analysis, we determine deposition rates for ZnO and Al₂O₃ and characterize the density of the constituent layers, comparing physical parameters as determined by XRR with ellipsometry and stylus profilometry measurements. We further elucidate the microstructure of the constituent layers using conventional and grazing incidence X-ray diffraction techniques.

Experimental Section

Atomic Layer Deposition Viscous Flow Reactor. An overhead schematic of the atomic layer deposition viscous flow reactor used for depositing the ZnO/Al₂O₃ nanolaminate films is presented in Figure 1. This ALD reactor is described in detail elsewhere.[29] Briefly, the reactor is constructed from off-the-shelf stainless steel components with VCR and Conflat all-metal seals. The samples are placed in a 60-cm long stainless
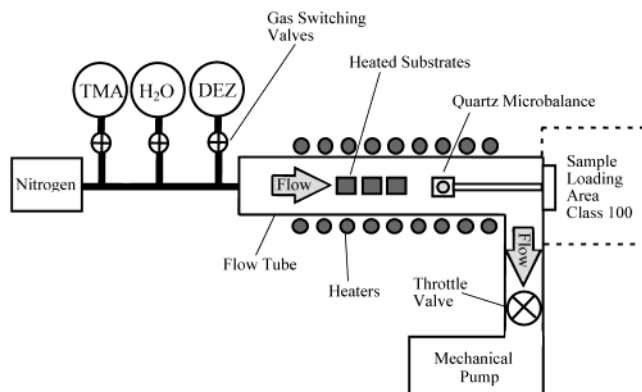

Figure 1. Schematic of atomic layer deposition flow reactor.

steel flow tube with a 3.5-cm inside diameter. Nitrogen gas supplied by three mass flow controllers continuously passes over the samples and into the Alcatel 2010 mechanical pump. The nitrogen carrier gas transports the reactive precursor gas pulses to the samples and also carries the unreacted precursors and reaction products out of the flow tube and into the mechanical pump. The total carrier gas flow is 200 cm³(STP) min⁻¹. A throttle valve above the exhaust pump is adjusted to maintain a pressure in the flow tube of 1 Torr. The flow tube walls are resistively heated to the desired ALD reaction temperature. Temperature stability is maintained by a proportional-integral-differential (PID) temperature controller which maintains ambient temperature within the flow tube at 177 °C.

The ZnO/Al₂O₃ nanolaminate films were deposited on *n*-doped Si(100) substrates. The Si(100) substrates are nearly atomically smooth. The sample substrates were cleaved from intact Si wafers into 1 × 1-in. squares. Degreasing was performed using a 15-min dip in Pirahna solution (70 mL H₂SO₄ and 30 mL 30% H₂O₂ solution), after which substrates were rinsed with distilled H₂O and dried under nitrogen gas. Inside of the sample loading clean area, the sample substrates were etched in clean room grade 5% HF/H₂O solution for 1 min to remove the native oxide, rinsed in Fischer Optima grade deionized water, and blown dry with filtered nitrogen gas prior to loading into the ALD reactor.

The ZnO films were deposited using alternating exposures to Zn(C₂H₅)₂ and H₂O,[24-27] while the Al₂O₃ films used alternating Al(CH₃)₃ and H₂O exposures.[14,28] The typical deposition temperature was 177 °C. At this temperature, the Al₂O₃ atomic layer deposition growth rate is maximized[14] and the ZnO ALD growth rate is nearly maximized.[26] The precursor needle valves on each reactant channel were adjusted to deliver ~0.1 Torr reactant gas pulses. Exposure times of 1- and 5-s purge times yielded an ALD cycle time of 12 s/cycle. These exposure and purge times were chosen conservatively to ensure saturation of the ALD surface reactions while preventing inadvertent mixing of the reactive gases.[29] Growth rates are measured in situ via a quartz crystal microbalance.

Atomic Force Microscopy. The ZnO, Al₂O₃, and ZnO/Al₂O₃ nanolaminate films were analyzed using a Thermomicroscopes Autoprobe CP scanning probe microscope. AFM images were acquired using intermittent contact mode at a scanning frequency of 1 Hz with Thermomicroscopes noncontact ultralever tips. The AFM measurements were performed in air, and 1 μm × 1 μm images were recorded using 512 scan lines and 512 pixels/scan line. Root-mean-square (rms) roughness was determined after raw images had been subjected to a second-order flattening procedure using Autoprobe CP image processing software.

X-ray Reflectivity/Thin Film Diffraction/Grazing Incidence X-ray Diffraction. X-ray reflectivity (XRR), high-angle thin film diffraction (XRD), and grazing incidence X-ray diffraction (GIXRD) measurements were collected using a

(17) Tanner, B.; Hudson, J. *IEEE Trans. Magn.* **1992**, *28*, 2736–2741.

(18) Stearns, D. G.; Gainese, D. P.; Sweeney, D. W.; Gullikson, E. M. *J. App. Phys.* **1998**, *84*, 1003–1028.

(19) Parratt, L. G. *Phys. Rev.* **1954**, *95*, 359–369.

(20) Wainfan, N.; Scott, N. J.; Parratt, L. G. *J. Appl. Phys.* **1959**, *30*, 1604–1609.

(21) Wainfan, N.; Parratt, L. G. *J. Appl. Phys.* **1960**, *31*, 1331–1337.

(22) Wormington, M. B.; D. K.; Tanner, B. K. *Mater. Res. Soc. Symp. Proc.* **1992**, *238*, 119–124.

(23) Wormington, M.; Panaccione, C.; Matney, K.; Bowen, D. *Philos. Trans. R. Soc. London A* **1999**, *357*, 2827–2848.

(24) Ott, A. W.; Chang, R. P. H. *Mater. Chem. Phys.* **1999**, *58*, 132–138.

(25) Lujala, V.; Skarp, J.; Tammenmaa, M.; Suntola, T. *Appl. Surf. Sci.* **1994**, *82/83*, 34–40.

(26) Yamada, A.; Sang, B.; Konagai, M. *Appl. Surf. Sci.* **1997**, *112*, 216–222.

(27) Yousfi, E. B.; Fouache, J.; Lincot, D. *Appl. Surf. Sci.* **2000**, *153*, 223–234.

(28) Higashi, G. S.; Fleming, C. G. *Appl. Phys. Lett.* **1989**, *55*, 1963–1965.

(29) Elam, J. W.; George, S. M. *Rev. Sci. Instrum.*, to be submitted for publication.

Philips X'Pert five-circle diffractometer. In all instances samples were aligned using a rigorous multistep alignment technique.

For XRR measurements, the incident beam (Cu Kα radiation, $\lambda = 1.5418$ Å) was conditioned by a Soller slit assembly, $1/32°$ divergence slit, and 10-mm Cu mask. The reflected X-ray intensity was collected by a scintillation counter, conditioned by a parallel plate collimator and a graphite monochromator with a 0.1 mm antiscatter slit immediately before the monochromator. Measurements were taken in a $\theta-2\theta$ geometry from $\theta = 0.1°$ to $\theta = 5.0°$ at 30 kV/20 mA tube power to maintain linearity in the detector response. Structural parameters were extracted from raw reflectivity data using REFS Mercury reflectivity autosimulation software (Bede Scientific Ltd.).[23] Simulations are based on solutions to the recursive formalism developed by Parratt[19] using the modifications of Nevot and Croce to simulate surface and interfacial roughness.[30] Autofitting is carried out by means of a genetic algorithm[31] with a logarithmic least-squares difference parameter (cost function) used to evaluate goodness-of-fit. Simulated parameters were considered final after the standardized cost function remained constant for over 10 000 iterations and after no less than 80 000 total iterations. The boundary conditions were set liberally to avoid local minima in the parameter space. Details of the fitting models are included in the discussion.

For XRD measurements, the incident beam (Cu Kα radiation, $\lambda = 1.5418$ Å) was conditioned by a Soller slit assembly, $1/4°$ divergence slit, and 10-mm Cu mask. The diffracted X-ray intensity was collected by a scintillation counter, conditioned by a parallel plate collimator and a graphite monochromator with no antiscatter slits. Measurements were taken in a $\theta-2\theta$ geometry from $2\theta = 10.0$ to $2\theta = 90.0°$ at 40 kV/45 mA tube power.

For GIXRD measurements, the incident beam (Cu Kα radiation, $\lambda = 1.5418$ Å) was conditioned using a parabolic mirror to provide a high-intensity quasi-parallel beam. The diffracted X-ray intensity was collected by a scintillation counter, conditioned by a parallel plate collimator and a graphite monochromator with no antiscatter slits. The incident beam angle was fixed at $\omega = 0.4$ to achieve a penetration depth of 1500−2000 Å, on the order of the thickness of the films under investigation. At higher incident angles significant scattering from the substrate was observed. Tube power was set to 45 kV/40 mA to achieve a stable incident beam, and the detector (2θ) axis was scanned from 15.0 to 90.0°.

Results/Discussion

X-ray Reflectivity Analyses. The deposition conditions for two sequences of multilayer samples is given in Table 1. The primary sequence ($j = 0-7$) consists of a series of seven samples with approximately constant total thickness but varying thickness in the repeating Al_2O_3/ZnO subunit. The multilayer labeled $j = 0$ consists of a single Al_2O_3/ZnO bilayer. Each successive multilayer consists of 2^j bilayers where the repeat unit thickness in each successive sample is half that of the previous sample, but the total multilayer thickness remains unchanged. To ease particular points of the discussion, these samples will be referred to as $j = 0$, $j = 1$, etc. as indicated in Table 1. The second sequence, labeled alphabetically, consists of multilayers in which the total repeat unit thickness is intended to be nearly constant while the relative proportion of Al_2O_3 and ZnO within the subunit is varied.

Reflectivity curves for $j = 0-7$ are shown in Figure 2. The low-frequency, high-intensity periodic maxima correspond to Bragg-like diffraction from the multilayer

Table 1. Deposition Conditions for Two Series of ZnO/Al₂O₃ Multilayers[a]

sample ID	multilayer recipe	Al_2O_3 layer thickness (Å)	ZnO layer thickness (Å)
$j = 0$	[500 c Al_2O_3, 300 c ZnO]	639.8	510.2
$j = 1$	[250 c Al_2O_3, 150 c ZnO] × 2	333.8	276.4
$j = 2$	[125 c Al_2O_3, 75 c ZnO] × 4	165.7	133.8
$j = 3$	[62 c Al_2O_3, 38 c ZnO] × 8	82.2	65.4
$j = 4$	[31 c Al_2O_3, 19 c ZnO] × 16	42.2	29.8
$j = 5$	[16 c Al_2O_3, 9 c ZnO] × 32	23.7	10.2
$j = 6$	[8 c Al_2O_3, 5 c ZnO] × 64	16.2 Å total repeat unit[b]	
$j = 7$	[4 c Al_2O_3, 2 c ZnO] × 128	923.1 Å total film thickness[c]	
A	[22 c Al_2O_3, 62 c ZnO] × 8	38.8	117.2
B	[42 c Al_2O_3, 50 c ZnO] × 8	62.9	95.6
C	[82 c Al_2O_3, 26 c ZnO] × 8	114.1	45.2

[a] One reaction cycle is equivalent to one complete binary reaction sequence. Average layer thicknesses reported above have been determined by computer simulation of experimental X-ray reflectivity curves. [b] For sample $j = 6$ the magnitude of the interfacial roughening is comparable to the constituent layer thickness, preventing reliable discrimination between Al_2O_3 and ZnO constituent layers. [c] For $j = 7$ no layering is observed.
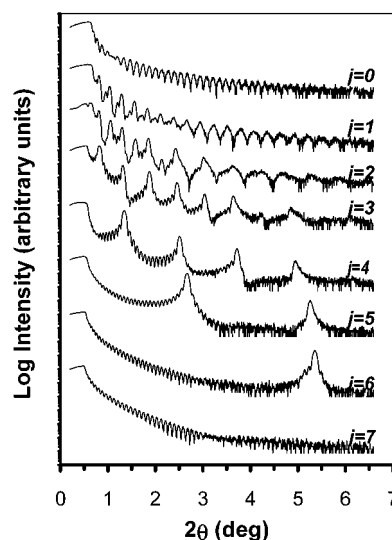

Figure 2. Overlay of X-ray reflectivity curves for multilayers $j = 0-7$ as defined in Table 1.

repeat unit (i.e., the Al_2O_3/ZnO bilayer). The thickness of the repeat unit can be determined using the Bragg relationship ($n\lambda = 2d \sin \theta$) for peaks occurring at $\theta > \sim 2°$. For smaller incident angles thicknesses must be determined using a form of Bragg's law appropriately modified to account for refractive effects which become significant for $\theta < \sim 2°$:

$$n\lambda = 2d(\sin^2 \theta - \delta)^{1/2} \tag{1}$$

where n is the diffraction order, λ is the wavelength of the incident X-rays, d is the repeat unit thickness, θ is the angular position of the Bragg reflection, and δ is the dispersive correction to the index of refraction for X-rays for the multilayer material.[21,32] The less-pronounced, high-frequency oscillations observable between Bragg reflections (so-called front-/back-reflections) can be similarly analyzed using eq 1, thereby providing a measure of the total multilayer thickness.

Qualitative analysis of the peak positions and profiles provides a wealth of preliminary information regarding the multilayer structure. No Bragg reflections are

(30) Nevot, L.; Croce, P. *Rev. Phys. Appl.* **1980**, *15*, 761−779.
(31) Holland, J. H. *Adaptation in Natural and Artificial Systems*, 2nd Ed.; MIT Press: Cambridge, MA, 1992.

(32) Wang, W.-H.; Bai, H. Y.; Zhang, M.; Zhao, J. H.; Zhang, X. Y.; Wang, W. K. *Phys. Rev.* **1999**, *B59*, 10811−10822.
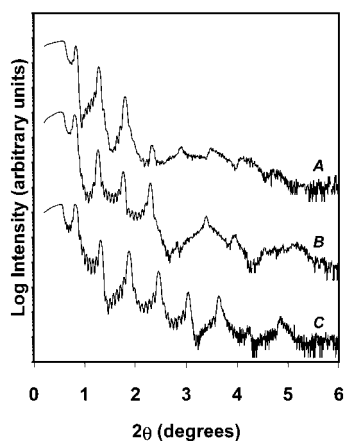
Figure 3. Overlay of X-ray reflectivity curves for multilayers A−C as defined in Table 1.

observed in two of the seven samples. The absence of Bragg peaks in $j = 0$ is trivial, in that $j = 0$ has no repeating subunit. For sample $j = 7$ no Bragg reflection is observed between $2\theta = 0$ and $2\theta = 15°$, though assuming a repeat unit thickness of 8−10 Å, one is expected around $2\theta \sim 11°$ (the reflectivity curve for $j = 7$ as shown in Figure 2 is abbreviated to $\sim 7°$ for clarity, beyond which point only noise is observed up to $2\theta = 15°$). The absence of this peak suggests that no true layering exists in $j = 7$, either due to complete inter-diffusion of the constituent layers during deposition or to interfacial roughness magnitudes which dwarf the constituent layer thicknesses. The position of the first-order Bragg reflection in $j = 6$ is well-matched with the second-order Bragg reflection in $j = 5$. Using Bragg's law as above, this relationship between peaks demonstrates to a first approximation that the bilayer thickness in $j = 6$ is half that of $j = 5$, as intended. Similar conclusions can be drawn regarding other pairs of successive multilayers (i.e., $j = 3$ and $j = 4$).

For a multilayer with x repeating subunits, Bragg peaks are coincident with front-/back-reflections of order mx (m an integer) such that $x − 1$ maxima are observed between Bragg peaks. The narrow breadth of the observed Bragg reflections is evidenced by the clear resolution of the front-/back-reflections of order $mx + 1$ and $mx − 1$ (i.e., those nearest to the Bragg reflections) in samples $j = 1–6$. The narrow breadth of the Bragg reflections is indicative of uniformity in the subunit thickness, that is, the thickness of each bilayer within the multilayer is well-matched. Bragg peak broadening is observed in higher order peaks in multilayers exhibiting multiple orders of Bragg diffraction.[17]

Reflectivity curves for the second set of samples, labeled alphabetically in Table 1, are given in Figure 3. Bragg peak positions are well-matched from sample to sample, indicating well-matched repeat unit thicknesses as intended. The most pronounced difference among the curves is the variation in the number of observable Bragg reflections. To a first approximation, a reflectivity curve may be thought of as a Fourier space representation of the multilayer electron density profile (EDP) normal to the sample surface. A multilayer with sharp interfaces, in which the EDP modulation resembles a square wave, must be described by multiple Fourier components evidenced by multiple orders of diffraction in the reflectivity curve. Though specular

reflectivity cannot explicitly distinguish between interfacial roughness and interdiffusion (i.e., a composition gradient), the attenuation of the Bragg-like peaks in the reflectivity curve provides a measure of interfacial quality encompassing both roughness and composition gradient effects. Among samples A−C, multilayers with thicker ZnO constituent layers exhibit fewer orders of reflection, indicating poorer interface definition. This observation is consistent with atomic force microscopy studies of single-component ALD ZnO films which indicate a correlation between increased ZnO surface roughness and ZnO layer thickness.[33] It should be noted that off-specular reflectivity[3,17,34,35] may be used to deconvolve roughness and composition gradient effects, though the interpretation of these data is less straightforward and will not be presented here.

Film density may be determined from the angle at which X-rays begin to penetrate the sample, the so-called critical angle for external reflection. For all known materials the index of refraction with respect to X-rays is slightly less than unity. The real part of the index of refraction for X-rays (neglecting absorption effects) may be written as

$$n_{\text{x-rays}} = 1 − \delta \qquad (2)$$

where δ is the dispersive correction to the refractive index (as in eq 1), a positive unitless parameter with a magnitude of $10^{-5}–10^{-6}$. Therefore, an X-ray beam impinging on a surface is passing from a region of higher refractive index (air) to one of lower refractive index. Below some critical incident angle (θ_c), dictated by Snell's law, the incident beam will be totally reflected from the surface. Beyond θ_c the X-rays will begin to penetrate the sample, and the collected intensity will begin to decrease. The position of the critical angle is related to δ as $\theta_c = (2\delta)^{1/2}$ and δ, in turn, is proportional to the bulk density of the material. Thus, a higher critical angle corresponds to a more dense material. The extraction of bulk density from δ requires an approximate knowledge of sample stoichiometry.[34]

Critical angle positions (see Figure 4) were determined analytically using Parratt's approximation that the critical angle is that angle at which the reflected intensity is half the totally reflected intensity.[19] A critical angle of $\theta \sim 0.33°$ is expected for a single-component crystalline ZnO film ($\rho = 5.61$ g/cm³), equivalent to the critical angle exhibited by $j = 0–2$. Thus in samples $j = 0–2$ the critical angle position is determined solely by the topmost ZnO layer. For $j > 2$ a lower critical angle position is observed ($\theta \sim 0.28°$) presumably representative of the average density of the multilayer stack. This presumption is born out by the trend observed in the critical angles of multilayers A−C (see Figure 5): samples with higher proportions of ZnO (the denser of the two bilayer components) show larger critical angles and therefore reflect a higher average density. A critical angle of $\sim 0.29°$ is expected for a single-component crystalline Al₂O₃ film ($\rho = 3.99$ g/cm³)

(33) Elam, J. W.; George, S. M. *Surf. Sci.*, to be submitted for publication.
(34) Holy, V.; Pietsch, U.; Baumbach, T. *High-Resolution X-ray Scattering from Thin Films and Multilayers*, 1st ed.; Springer-Verlag: Berlin, 1999.
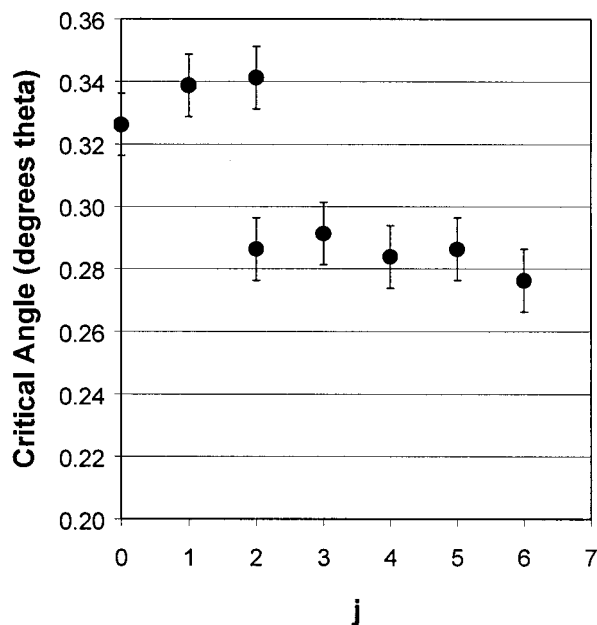(35) Holy, V.; Baumbach, T. *Phys. Rev. B* **1994**, *49*, 10668−10676.

Figure 4. Position of the critical angle for total external reflection for each multilayers $j = 0-7$ as defined in Table 1. Sample $j = 2$ exhibits two critical angle features.
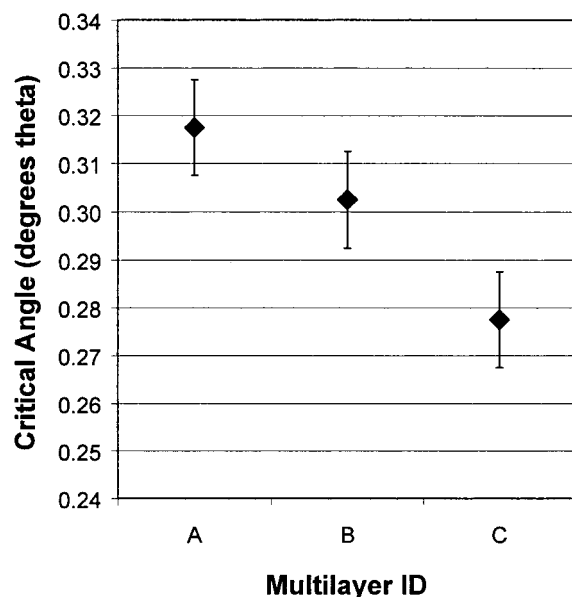

Figure 6. Schematic of physical model employed in simulating reflectivity curves.

Figure 7. Comparison of experimental reflectivity curve (solid line) with simulated reflectivity curve (open circles) for $j = 2$.

Figure 5. Critical angles for multilayers A–C (as defined in Table 1). The critical angle decreases as the relative proportion of ZnO in the ZnO/Al$_2$O$_3$ bilayer subunit decreases.

larger than the observed critical angles for $j > 2$. Since the observed critical angle represents an average density intermediate between the ZnO and Al$_2$O$_3$ layer densities, the density of the Al$_2$O$_3$ layer must be smaller than the bulk value.

More detailed structural parameters, such as the density of buried layers or relative amounts of individual constituents within the multilayer repeat unit, have more subtle effects on the overall reflectivity curve and are best determined through appropriate computer simulation. Extraction of meaningful structural parameters through computer simulation requires the creation of a physical model that reasonably approximates the system under investigation. Our approach to devising a physical model was to use the simplest model which
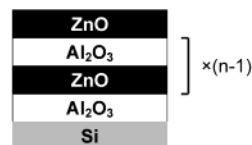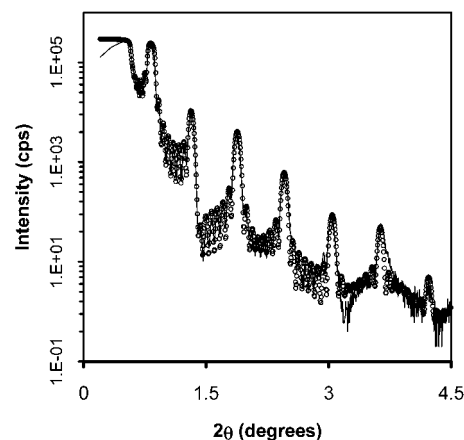
would still provide a reasonable fit to experimental data. Samples $j = 0$ and $j = 1$ were successfully modeled using two (ZnO/Al$_2$O$_3$ on Si) and four (ZnO/Al$_2$O$_3$/ZnO/Al$_2$O$_3$ on Si) discrete layers, respectively. Sample $j = 7$, in which no layering was observed, was modeled as a single layer of composition ZnO–Al$_2$O$_3$ with a thin ZnO surface layer. For the remaining multilayer samples, models containing discrete layers were no longer practical. The simplest conceivable models of the form (ZnO/Al$_2$O$_3$)$_n$, in which the bilayer subunits are assumed to be identical, failed to produce reasonable fits. Models of the form Si–Al$_2$O$_3$–(ZnO–Al$_2$O$_3$)$_{n-1}$–ZnO (as shown in Figure 6) were devised in order to preserve the uniqueness of the bottom Si/Al$_2$O$_3$ interface and the topmost ZnO/air interface. These models were found to produce excellent fits with experimental reflectivity curves, as shown in Figure 7. At higher angles some slight discrepancy between experiment and simulation becomes evident, partly because the reflectivity signal is nearer the noise level. In addition, our model requires that all ZnO/Al$_2$O$_3$ bilayer subunits have identical structural parameters; thus peak broadening associated with bilayer nonuniformity is not accounted for.

Density parameters as determined by computer simulation show the density of the ZnO layers to be within $\pm 5\%$ of bulk ZnO density (5.61 g/cm^3). Al$_2$O$_3$ density is found to be 3.1 ± 0.1 g/cm^3, or $77 \pm 3\%$ of expected bulk density (3.99 g/cm^3), consistent with the previous qualitative analysis of critical angle position. These results are in clear quantitative agreement with the densities of similarly prepared single-component films determined by quartz crystal microgravimetry and stylus profilometry analysis, 5.52 and 3.15 g/cm^3 for ZnO and Al$_2$O$_3$ respectively.[33] Note that the QCM/profiler and XRR densities determined for Al$_2$O$_3$ are appreciably lower than the density previously reported for similarly prepared Al$_2$O$_3$ films as determined by ellipsometry.[14]

Root-mean-square roughness parameters for $j = 0-3$ are reported in Table 2. For $j > 3$ the roughness

Table 2. Root-Mean-Square Roughness Parameters for Samples $j = 0-3$ As Determined by Computer Simulation of X-ray Reflectivity Curves[a]

sample ID	rms surface roughness (Å)	sample ID	rms surface roughness (Å)
$j = 0$	36.0	$j = 2$	18.1
$j = 1$	21.1	$j = 3$	14.2

[a] For $j > 3$ the roughness approximation employed by the simulation software is no longer rigorously correct in that the magnitude of the rms roughness is comparable to the thickness of the topmost layer.
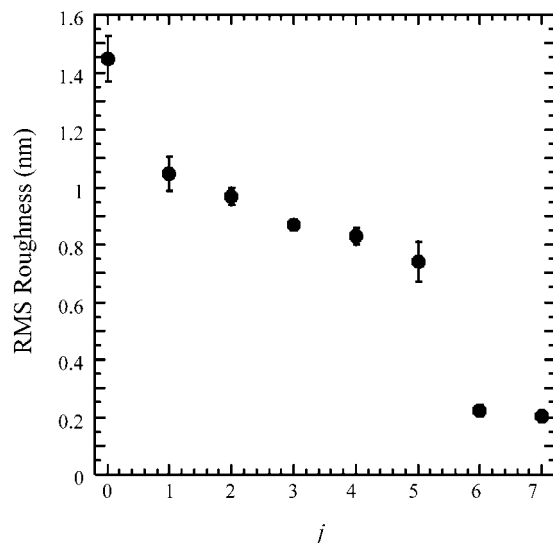
Figure 8. Rms surface roughness of multilayers $j = 0-7$ as determined by atomic force microscopy. The sharp decrease between $j = 5$ and $j = 6$ corresponds to the disappearance of crystalline ZnO intensity observed by GIXRD.

approximation employed by the simulation software is no longer rigorously correct, in that the thickness of the constituent layers is on the order of the interfacial roughness.[30,36] Atomic force microscopy measurements of these nanolaminates show a similar decrease in roughness as the number of bilayers increases, as shown in Figure 8.[37] We emphasize that direct quantitative comparison of rms roughness as determined by AFM and XRR is inappropriate as the two techniques describe the roughness over drastically different length scales.[38]

Thickness parameters extracted from reflectivity curves by computer simulation are reported in Table 1. Analysis of constituent layer thicknesses for $j = 0-4$ and multilayers A–C show linear deposition rates corresponding to 1.71 Å/reaction cycle ($R^2 = 0.997$) and 1.28 Å/reaction cycle ($R^2 = 0.999$) for ZnO and Al₂O₃ respectively. Ellipsometry and stylus profilometry measurements for similarly prepared single-component Al₂O₃ films show a deposition rate of 1.29 Å/reaction cycle, in clear quantitative agreement with XRR.[33] Analysis of single-component ZnO films by the same techniques show that ZnO deposition rate increases from an initial rate of ~1.5 Å/cycle to a constant rate of 2.01 Å/cycle beyond 1000 reaction cycles. The XRR
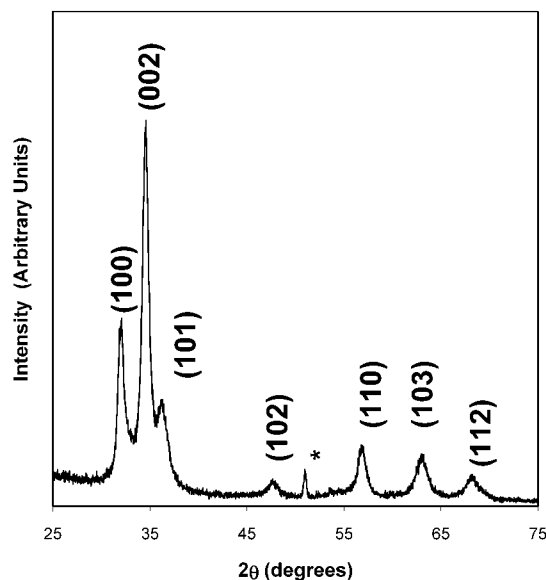
Figure 9. GIXRD pattern for $j = 1$. All peaks correspond to ZnO reflections from ICDD file 36-1541. The peak marked with an asterisk is attributed to the substrate, as discussed in the text.

determined deposition rate of 1.71 Å/reaction cycle agrees with the 1.5–1.9 Å/cycle observed over the range of 0–300 ZnO reaction cycles by ellipsometry and stylus profilometry. The repeat unit thicknesses and/or total film thicknesses for samples $j = 5-7$ suggest a negative deviation from the rates determined for $j = 0-4$. The simulated thicknesses for sample $j = 5$ suggest that the ZnO layer is thinner than expected. This discrepancy is consistent with the observation that ZnO deposition is less favorable at an Al₂O₃ surface, hindering the ZnO growth rate for the first few layers.[39]

Microstructural Characterization. High-angle thin film diffraction measurements were made to elucidate the nature of the ordering in the individual layers. Several critical peaks were obscured by reflections from the Si substrate. These substrate peaks, coupled with the low intensity and peak broadening of characteristic of thin film diffraction peaks, prevented any certain analysis of XRD data. To attenuate substrate effects, grazing incidence X-ray diffraction (GIXRD) was employed. In a GIXRD measurement, the sample is held at a small fixed angle relative to the incident beam while the detector is scanned over a wide range. The incident beam is collimated by a multilayer mirror to eliminate the need for a purely focusing geometry. The penetration depth of the X-rays can be controlled by judicious choice of incident angle.[40,41]

GIXRD measurements for sample $j = 1$ is shown in Figure 9. Comparison with ICDD powder files provides unambiguous identification of polycrystalline ZnO. No diffraction from an AlO$_x$ phase is observed. The presence of an amorphous Al₂O₃ layer is consistent with the low densities observed by X-ray reflectivity and ellipsometry.[14] By the same token, the good agreement between

(36) Ritley, K. A.; Just, K.-O.; Schreiber, F.; Dosch, H.; Niesen, T. P.; Aldinger, F. *J. Mater. Res.* **2000**, *15*, 2706–2713.

(37) Elam, J. W.; Sechrist, Z. A.; George, S. M. *Thin Solid Films*, submitted for publication.

(38) Chason, E.; Falco, C. M.; Ourmazd, A.; Schubert, E.; Slaughter, J. M.; Williams, R. S. *Mater. Res. Soc. Symp. Proc.* **1993**, *260*, 203–239.

(39) Yousfi, E. B.; Weinberger, B.; Donsanti, F.; Cowache, P.; Lincot, P. *Thin Solid Films* **2001**, *387*, 29–32.

(40) Lim, G.; Parrish, W.; Ortiz, C.; Bellotto, M.; Hart, M. *J. Mater. Res.* **1987**, *2*, 471–477.

(41) Bowen, D. K.; Wormington, M. *Adv. X-ray Anal.* **1993**, *36*, 171–184.
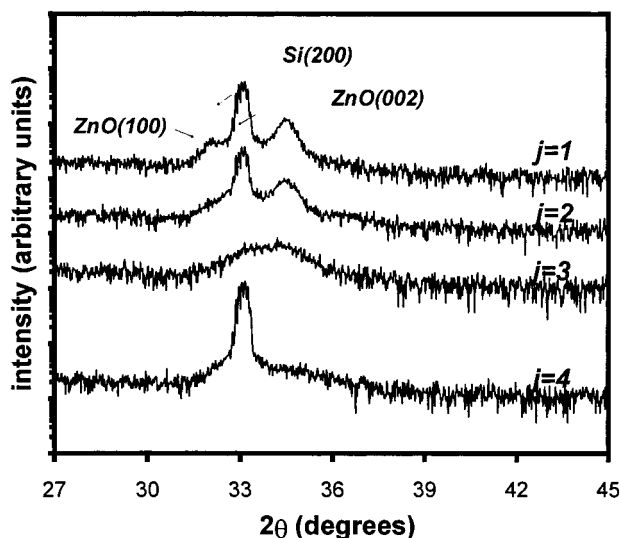
2282 *Chem. Mater., Vol. 14, No. 5, 2002*

Jensen et al.

**Figure 10.** Detail of conventional high-angle thin film diffraction measurements of ZnO/Al$_2$O$_3$ multilayers.

Figure 11. Trend in GIXRD peak breadths, samples $j = 1$ (top) to $j = 7$ (bottom). Sharp peaks ~51 and 52° are attributed to the substrate.

ZnO layer density and bulk ZnO density are consistent with crystalline ZnO. An unindexed peak at ~51° was observed in nearly all scans. When the penetration depth of the incident X-rays was increased (by increasing the incident angle), the intensity of this peak increased dramatically, while the assigned ZnO peaks were found to decrease slightly. On this basis the peak at ~51° was assigned to the substrate.

The high-angle thin film diffraction data were reexamined in light of the identification of crystalline hexagonal ZnO. The most prominent reflection which was readily differentiable from the substrate was the ZnO(002) reflection. ZnO films prepared on glass substrates at similar temperatures have been observed to exhibit strong ZnO(100) preferred orientation normal to the sample surface.[26,27] The ZnO layers within the multilayers are grown on amorphous Al$_2$O$_3$ layers and show preferred ZnO(002) orientation. Thus, ZnO layer growth appears to be substrate-sensitive, not surprising given the integral role of the surface structure in the deposition process.

The breadth of the observed ZnO(002) peak increases with increasing j (see Figure 10), indicating a decrease in ZnO grain size in the direction normal to the sample surface. This trend is not surprising, given that ZnO grain size in the direction normal to the sample surface is necessarily limited by the thickness of the constituent ZnO layer. Given the low intensity of the peaks and convolution of the broader peaks with the proximate ZnO(100) and quasi-forbidden Si(002) reflection, no quantitative analysis of grain size was attempted.

A similar trend in peak breadths was observed in the GIXRD patterns (see Figure 11). Unlike thin film XRD which probes diffraction from atomic planes parallel to the sample surface, a GIXRD pattern represents reflections from atomic planes perpendicular to the sample surface. The broadening of the peaks can be interpreted as decreasing ZnO grain size in the general plane of the sample. For $j > 5$ the ZnO peaks disappear completely and the growth of a broad peak at ~55° is observed. The absence of the ZnO peaks cannot be the result of complete ZnO/Al$_2$O$_3$ mixing in that Bragg reflections corresponding to ZnO/Al$_2$O$_3$ bilayers are still observed
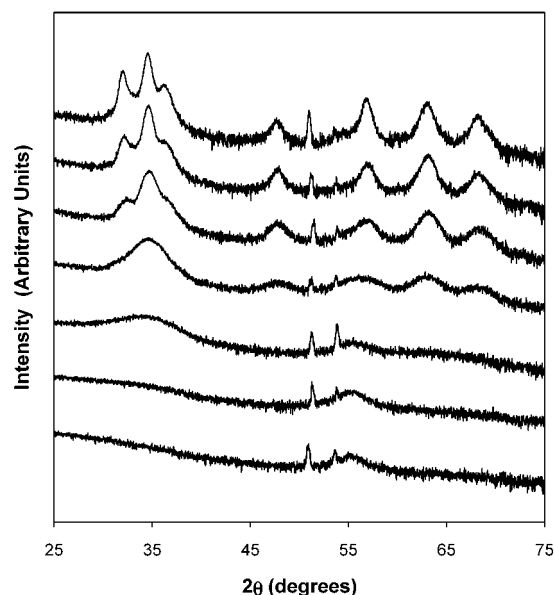
in $j = 6$. AFM analysis of the multilayers shows a sharp decrease in rms surface roughness between $j = 5$ and $j = 6$ as shown in Figure 8. Taken together these data suggest that ZnO crystallization is completely suppressed below some critical number of deposition cycles (between 5 cycles and 9 cycles).

Conclusions

X-ray reflectivity has been used to provide efficient and accurate characterization of a series of ZnO/Al$_2$O$_3$ multilayer films prepared by atomic layer deposition. Structural parameters determined by computer simulation of reflectivity data have been used to measure the rate of deposition for Al$_2$O$_3$ and ZnO and to quantify observations regarding layer density and surface roughness. Deposition rates and layer densities as determined from first principles by XRR are in clear quantitative agreement with rates and densities measured by alternate methods on single-component films. Further microstructural characterization using conventional and grazing-incidence X-ray diffraction shows that ZnO film thickness limits grain growth in all directions and elucidates a probable substrate dependence on the preferred orientation of polycrystalline ZnO by ALD. The absence of any diffraction from Al$_2$O$_3$ demonstrates the layers are amorphous, consistent with the low densities determined by X-ray reflectivity.